Winter 1-2020

Numerical investigation of Darrieus wind turbine with slotted airfoil blades

Ahmed Elbaz
The British University in Egypt, ahmed.elbaz@bue.edu.eg

Omar Sherif Mohamaed
The British University in Egypt, omar.mohamed@bue.edu.eg

Ahmed Abdelhamid Ibrahim
The British University in Egypt, ahmed.abdelhamid@bue.edu.eg

Ahmed Khaled Etman
The British University in Egypt, ahmed.khaled.etman@gmail.com

Amr A. Abdelfattah
The British University in Egypt, amr.abdelkader@bue.edu.eg

Energy Conversion and Management: X 5 (2020) 100026

Contents lists available at ScienceDirect

Energy Conversion and Management: X

journal homepage: www.journals.elsevier.com/energy-conversion-and-management-x

Numerical investigation of Darrieus wind turbine with slotted airfoil blades

Omar S. Mohamed, Ahmed A. Ibrahim, Ahmed K. Etman, Amr A. Abdelfatah, Ahmed M.R. Elbaz*

Department of Mechanical Engineering, Faculty of Engineering, The British University in Egypt, El Sherouk City, Suez-Cairo Desert Road, Cairo 11837, Egypt

ARTICLE INFO

Keywords:
Vertical axis wind turbine (VAWT)
Self-starting
Computational fluid dynamics (CFD)
H-type rotor
Flow separation
Slotted airfoil

ABSTRACT

Low starting torque is considered as one of the major drawbacks of Darrieus type vertical axis wind turbine (VAWT). Design optimization to overcome this problem by modifying the airfoil geometry has received great attention by the wind energy community. Moreover, efforts have been directed towards augmenting the power coefficient of the turbine. In the present work, the effect of employing slotted airfoil as turbine blade on the performance and starting characteristics has been investigated. The slot parameters; slot location, angle of inclination, and dimensions, were optimized for NACA 0018 airfoil which is commonly used in Darrieus turbines. The flow over the turbine was modelled using ANSYS-FLUENT code. The main observations of the present study show that the VAWT with slotted Airfoil (SA) has a lower optimum tip speed ratio (TSR) compared with the Baseline (BL) turbine. This is associated with the ability to generate higher torque at lower rotational speeds. The analysis of the aerodynamic behavior of the SA turbine shows that the airfoil slot delays the separation at high angles of attack, and therefore improves the torque and power coefficient at low TSR.

1. Introduction

Research interest in the Darrieus type vertical axis wind turbine (VAWT) has been growing rapidly in the last few years considering its relatively low cost, ease of maintenance, and noiselessness. The main research interest in Darrieus turbine aerodynamics is currently concerned with finding ways to enhance the power coefficient, starting torque, and power density [1–3]. Hybridization of Darrieus and Savonius turbine has been investigated by various researchers recently. It was concluded that hybrid designs could enhance the self-starting capabilities of Darrieus turbine [4–6]. Other researches aimed at enhancing the performance of the turbine's airfoil. The airfoil can be defined as the cross section of a body located in the air-stream to generate aerodynamic forces. Airfoils are found in propellers, hydrofoils, aircrafts, and wind turbines. In wind turbines, the airfoil is a vital element, as it converts the kinetic energy of the wind into mechanical energy.

Innovations in the airfoil profile optimization have been carried out in numerous works. Bionic airfoil was investigated resulting in higher lift coefficient, better stalling characteristics, and higher power coefficient when employed in horizontal type wind turbine, compared to the clean airfoil [7]. Sengupta et al. [8] examined the effect of airfoil shape on the performance of VAWT and concluded that using cambered airfoils results in lower negative torque, which enhances the overall turbine efficiency. Scungio et al. [9] examined an alternative design approach for the VAWT rotor in which a pair of airfoils were installed consecutive to each other. Flow deflector near the trailing edge of the suction side can be an effective separation control technique [10]. Augmentation in lift force relative to drag force has been achieved by a modified chambered airfoil introduced by Al-Shohani et al. [11].

Other performance enhancing techniques of VAWT which have been reported in the literature include adding flow modifying structures such as deflectors and concentrators. Wang et al. [12] studied a passive way of delaying flow separation by adding leading edge slat. The study showed that the separation point was shifted to higher angle of attack (AoA). Wong et al. [13] studied the effect of adding an upwind deflector for Darrieus VAWT. Their study showed that the deflector accelerates the upwind speed by about 25% which augments the performance at low wind speeds. Lee et al. [14] investigated experimentally the effect of truncated-cone-shaped wind gathering device on Darrieus type turbine self-starting capabilities. They concluded that the maximum averaged static torque coefficient increased by 24.2% due to the optimized wind gathering device.

Darrieus Hydrokinetic turbine has been experimentally investigated by [15]. They concluded that low solidity turbines could have difficulty to run at low TSRs. Another experiment has been conducted by Patel et al. [16] to augment the performance of hydrokinetic Darrieus turbines by blocking the flow over the retarding blades which mainly

* Corresponding author.
E-mail addresses: omar118091@bue.edu.eg (O.S. Mohamed), ahmed118790@bue.edu.eg (A.A. Ibrahim), PG.ahmed91810011@bue.edu.eg (A.K. Etman), amr.abdelkader@bue.edu.eg (A.A. Abdelfatah), ahmed.elbaz@bue.edu.eg (A.M.R. Elbaz).

https://doi.org/10.1016/j.ecmx.2019.100026
Received 9 August 2019; Received in revised form 5 November 2019; Accepted 6 November 2019
Available online 15 November 2019

Nomenclature

A	Rotor swept area [m^2]
C	Chord length [m]
C_D	Drag coefficient [–]
C_P	Power coefficient [–]
C_T	Torque coefficient [–]
C_L	Lift coefficient [–]
D	Turbine diameter [m]
H	Rotor height [m]
L	Slot position from leading edge [m]
N	Rotational speed [rev/min]
n	Number of blades [–]
P	Output power [W]
Pc	Pressure coefficient [–]
p	Pressure [N/m^2]
R	Tip radius of turbine [m]
R_e	Reynolds number [–]
T	Output torque [N.m]
V_∞	Wind speed [m/s]
W_1	Slot outlet width [m]
W_2	Slot inlet width [m]
y^+	Dimensionless distance from solid surface [–]
β	Slot inclination angle [Deg]
λ	Tip speed ratio [–]
ν	Kinematic viscosity [m^2/s]
ρ	Air density [kg/m^3]
θ	azimuth angle
ω	Angular speed [rad/s]

produce negative torque. The study concluded that the power coefficient could be enhanced by 188% if specific orientation of blocking plate is maintained.

The effect of airfoil leading edge serrations was studied numerically by Lositaño et al. [17]. They concluded that, at high tip speed ratio, the cambered tubercle leading edge blade encounters a sudden drop in torque coefficient during the upwind half cycle. This behavior was attributed to a sudden rise in the drag force. A comparative study between leading edge serrated blade VAWT and the conventional blade VAWT was carried out by Wang et al. [18,19]. They concluded that flow separation was significantly delayed, which shows a remarkable augmentation of the power coefficient at low tip speed ratios.

The results obtained for VAWT by adding a dimple on the airfoil were reported by Sobhani et al. [20]. Using various geometries and locations of the dimple, it was observed that adding a circular dimple on the leading edge of the pressure side resulted in a significant improvement of the power coefficient because of the reduction in flow velocity caused by the trapped air in the leading edge gap, which increases the pressure on this side of the blade. Zhu et al. [21] also conducted a numerical investigation of the VAWT applying both dimples and gurney flap to the turbine blade at different solidity ratios. The study concluded that both Gurney flap and dimple with Gurney flap on the suction side could enhance the power coefficient of the Darrieus turbine. They concluded that the Gurney flap enhances the power coefficient at low TSR, while combined dimple with Gurney flap could enhance the aerodynamic performance at higher TSR [22]. Bianchini et al. [23] also investigated numerically the influence of Gurney flap on the aerodynamic performance of the Darrieus turbine. They concluded that locating the flap on the suction side generates strong oscillations in the turbulent kinetic energy and vortex shedding phenomenon, hence, they recommended to install the flap on the pressure side of the blade. This is in contradiction to the recommendations reported in [21] to install the Gurney flap on the suction side. The main reason of this contradiction is believed to be that each group of researchers presumed that the Gurney flap variables e.g. flap orientation and length are independent of the turbine variables, e.g. TSR and solidity.

Adaptive trailing edge flap effect on airfoil stall performance was optimized by Hao et al. [24]. In their study, the performance of the airfoil was assessed by observing the effect of changing flap length, flap location, and flap angle on the total lift coefficient. Sengupta et al [25] concluded that, at low wind speeds, curvature signature of unsymmetrical airfoil profile could enhance the performance of Darrieus turbine. Ma et al. [26] optimized the airfoil profile using an automatic geometry generation technique and approached a significant enhancement in torque coefficient at low TSR. Zhong et al. [27] added a cylindrical rod near to the blade's leading edge to delay dynamic stall of Darrieus VAWT. The numerical results showed enhancement of the power coefficient at low TSR. The rod effect was found to maintain the

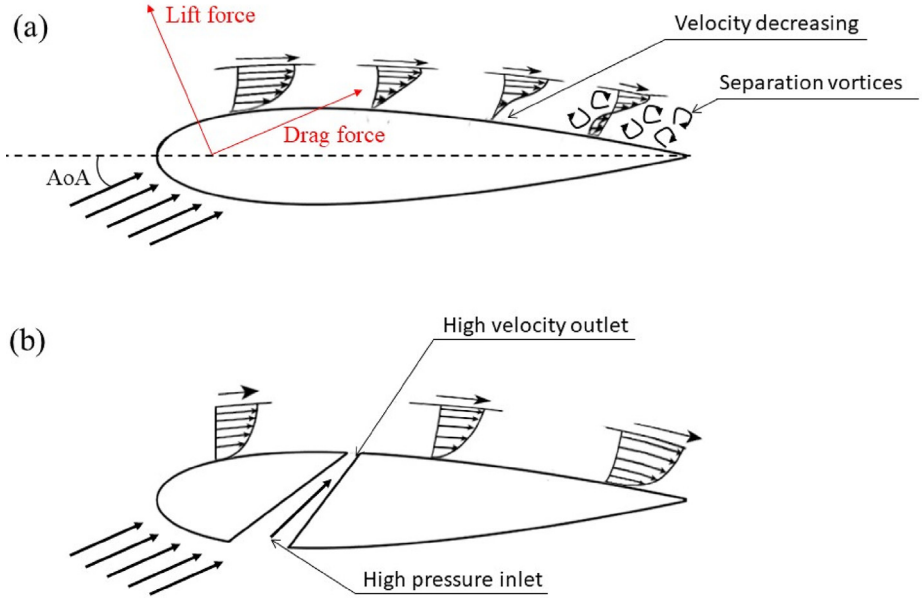

Fig. 1. Hypothetical schematic representation of flow over airfoil; a- Clean airfoil, b- airfoil with slot.

flow attached to the blade for wider range of AoA, and this effect declined gradually with increase of TSR due to decrease of AoA range.

Using a slotted airfoil is considered as a passive method of boundary layer control, which was first introduced to enhance the lifting characteristics of airplane wings [28,29], air compressor blades [30], and helicopter blades [31]. Such slot extends from the pressure side of the airfoil to the suction side. Many parameters affect the slot performance in terms of boundary layer control on the suction side such as: slot width, slot location, inclination angle and slot shape. Due to the difference in pressure between the pressure side and suction side, the air flows through the slot to inject momentum into the boundary layer of the suction side. Narsipur et al [32] discussed the applicability of slotted airfoil in wind turbine blades. Belamadi et al. [33] provided detailed study of the influence of single slot geometrical parameters on the lift and drag coefficients of a NREL S809 airfoil. They also discussed the applicability of their results to produce possible enhancement of the performance of VAWT but did not report any results of the application. This recommendation emerged from the favorable increase of glide ratio (ratio between lift and drag coefficients) at wider range of angles of attack using the optimized slot parameters. They investigated two shapes of the airfoil slot, the straight shape and the convergent shape. The convergent shape with area ratio between slot inlet and outlet of 4, where the slot outlet is located at 50% of the chord with inclination angle of 60° produced the best performance. Although the maximum glide ratio was marginally increased, however, the separation was eliminated up to angle of attack of 20°.

The present investigation aims to study the effect of employing the slotted airfoil in VAWT using NACA 0018 [34] blades. Two dimensional numerical simulations were performed for different slot configurations aiming to obtain the highest glide ratio at wide range of angles of attack. The optimized slot geometry was applied to the H-type Darrieus type VAWT at a wide range of tip speed ratio (TSR). The results show the effect of the airfoil slot on the torque and the power coefficients of the turbine, compared with the original airfoil blade results. Moreover, a detailed analysis of the turbine behavior is presented based on the details of the aerodynamic field results of both types.

2. The slotted airfoil

The Darrieus type wind turbine is a lift-type VAWT, where the lift force exerted on the turbine blade is of main concern. Basically, the lift and drag forces are generated due to difference in pressure between the airfoil upper and lower surfaces. Negative pressure is produced on the suction side of the airfoil, while positive pressure is generated on the pressure side. This scenario persists for small angles of attack. At higher angles of attack, flow separation occurs due to the positive pressure gradient towards the trailing edge of the airfoil. Fig. 1 shows the typical flow behavior along an airfoil section with initiating flow separation at the trailing edge for a conventional airfoil (Fig. 1-a) and a slotted airfoil (Fig. 1-b). The slot, as depicted in Fig. 1-b, extends from the pressure side (lower side) to the suction side (upper side). Due to the difference in pressure between the two sides, a jet flow is formed through the slot, and high momentum is injected into the boundary layer of the upper surface. The effect of this jet is to eliminate separation at mild angles of attack and extend the high lift range of the airfoil.

In order to optimize the geometrical parameters of the slot, a numerical study was performed. The NACA 0018 airfoil [34] was used as a baseline geometry. Fig. 2 shows the basic geometrical parameters of the slotted airfoil, which are:

1. The location of the midpoint of the slot from the leading edge (L).
2. The slot outlet width (W_1).
3. The slot inlet width (W_2).
4. The slot inclination angle (β).

The slot outlet edge must be curved such that the jet flow is injected parallel to main flow direction at the point of injection. This is essential in order to enhance the momentum of the boundary layer. Failing to do so causes flow separation at the slot outlet which consequently reduces the lift force.

The baseline airfoil used in the present work is NACA 0018 with a chord length (C) of 0.47 m. Table 1 summarizes the tested parameters of the airfoil slot, where in all cases W_2/W_1 took a value of 4.0 as recommended in [33]. Two values of slot angle were tested: 45° and 60°. These angles were tested for L/C ranging from 15% to 35% and W_1/C ranging from 2 to 3.5%.

3. Numerical methodology for airfoil simulations

Fig. 3 shows the computational domain used for the airfoil simulations. A C-domain type was used to enable easier variation of the angle of attack by manipulating the incoming flow direction through the semi-circular inlet boundary. The domain dimensions are presented in terms of chord length C. Table 2 shows the predicted ratio between lift coefficient and drag coefficient of the airfoil for different domain sizes in the upstream and downstream sides of the airfoil, using 80C domain width in the cross stream direction. As can be seen in the table, the domain size affects the computed results. Small domain size restricts the flow development and affects the obtained results. Increasing domain size beyond domain #4 has very little effect on the results. Therefore, domain #4 dimensions were selected to ensure domain independent results for an isolated airfoil.

The numerical domain was discretized into small control volumes. The grid density was tested to obtain grid independent results as shown in Table 3. The selected grid (grid # 4) for the isolated airfoil case had approximately 140,000 nodes and 40 inflation layers around the airfoil wall. The grid had maximum skewness below 0.6. The y^+ value of the first grid point was below one in order to apply enhanced wall treatment k-ε or k-ω SST turbulence models. ANSYS-Fluent flow solver was used [41] to carry out flow simulations. Fig. 4 shows typical details for the airfoil grid.

Pressure based solver was utilized while the pressure-velocity coupling was handled using coupled algorithm. Second order upwind discretization scheme was utilized for all URANS and turbulence equations, which guarantees minimum numerical diffusion. The convergence of the simulations was assessed by a low residual level of 10^{-5}.

4. Results of baseline and slotted airfoils

Selecting the appropriate turbulence model which achieves the best agreement with experimental results is a crucial step to guarantee reliable results. Three turbulence models were examined in this study; namely: the Realizable k-ε model [35], the shear stress transport k-ω SST model [36] and k-ε RNG model [37]. Computed variation of lift coefficient (C_L) with angle of attack (AoA) using these models are

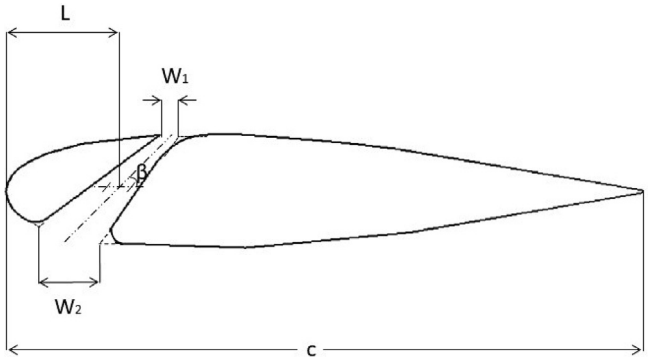

Fig. 2. Geometrical parameters of the slotted airfoil.

Table 1
Test cases of slotted airfoil.

Configuration#	1	2	3	4	5	6	7	8	9	10
W_1/C (%)	2	2.5	2.5	2.5	2.5	3	3	3	3.5	3.5
L/C (%)	20	25	15	30	35	15	20	25	15	30
β (degree)	45	45	60	60	60	45	45	45	45	45

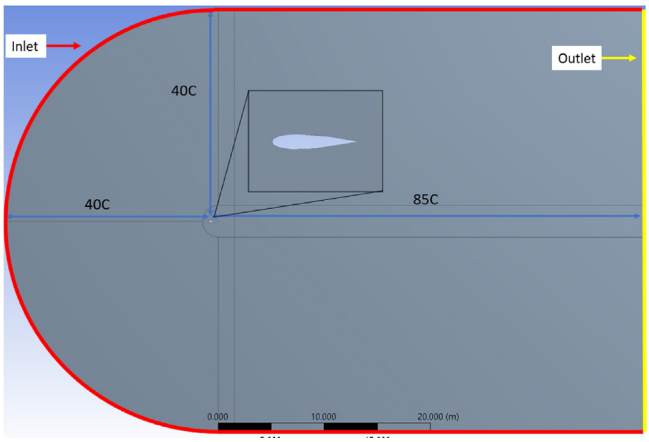

Fig. 3. Details of the airfoil computational domain.

Table 2
Predicted glide ratio for the Tested domains.

Domain #	Downstream distance	Upstream distance	Resulted C_L/C_D
1	25C	10C	6.180
2	45C	20C	5.936
3	65C	30C	5.897
4	85C	40C	5.876
5	110C	50C	5.877
6	125C	60C	5.878

Table 3
Predicted glide ratio for different grids.

Grid #	Element size on the airfoil [m]	# of inflation layers	# of nodes	Resulted C_L/C_D
1	0.00235	10	74,922	6.071
2	0.001567	20	94,424	6.021
3	0.001175	30	122,678	5.956
4	0.00094	40	135,796	5.934
5	0.000783	50	151,714	5.904
6	0.000671	60	204,843	5.906

compared in Fig. 5 with the experimental results of [38] at Re = 250,000. Both the realizable k-ε model and the RNG model show better agreement with the experimental measurements. The k-ω SST model predictions show too fast separation where the lift coefficient starts to drop earlier than the experimental data. The peak value of the C_L is also underpredicted by the k-ω SST model. Therefore, the realizable k- ε turbulence model is selected and used for slotted airfoil simulations. The highest error of this model occurs at AoA = 20°. However, at all other AoA, the error does not exceed 14%.

The benefit of using the airfoil slot concluded by Belamadi [33] was to widen the zone where the glide ratio is high compared to the baseline airfoil. Therefore, two characteristic parameters are proposed to assess the performance of the slotted airfoil. The first parameter is the maximum glide ratio. The second parameter is the range of the angles of attack through which the glide ratio is higher than half its maximum value. These two parameters are explained in Fig. 6. Table 4 shows the obtained results for the ten tested cases. The maximum glide ratio results show that there is no significant difference for all slotted airfoil configurations compared with the baseline airfoil. In fact, the slotted airfoil cases have slightly lower glide ratio compared with the baseline airfoil. However, the baseline airfoil range of 50% glide ratio is 14°while most of the slotted airfoil cases achieve higher range. Cases 6 and 9, particularly, show the highest glide ratio and range. Therefore, case 9 was selected for application in the Darrius wind turbine since its range occurs at higher angles of attack.

Figs. 7–9 show comparison between slotted airfoil results (case 9) and the baseline airfoil results in terms of variation of the lift coefficient, the drag coefficient, and the glide ratio with the angle of attack. As can be observed, there are significant differences in the lift and drag coefficients between the slotted airfoil and the baseline airfoil for AoA > 12°, at which the baseline airfoil is subjected to separation, leading to a fast drop of the lift coefficient and increase of the drag coefficient. On the other hand, the slotted airfoil shows a continuous rise of the lift coefficient, while the drag coefficient stays at low values. This indicates that flow separation is delayed for the slotted airfoil. The separation starts to appear for AoA > 23° for the slotted airfoil, where the lift coefficient starts to decrease while the drag coefficient rises faster. As shown in Fig. 9, the peak glide ratio is slightly lower for the slotted airfoil than that of the baseline airfoil. The AoA of the peak glide ratio of the slotted airfoil is 14° while that of the baseline airfoil occurs at an AoA of 12°. The C_L at this angle is 1.25 which is 83% of the maximum C_L. The corresponding C_L value of the baseline airfoil is 75% of the peak C_L. This is in favour of the slotted airfoil since it means that selecting the angle of attach of the peak glide ratio results in closer lift coefficient to the peak lift coefficient and correspondingly smaller airfoil area is needed for the same lift force.

The range of 50% peak glide ratio is shown in Fig. 9 to be 6°wider using the slotted airfoil, compared with the baseline airfoil. It could be noticed that at AoA = 0° the flow around the slotted airfoil is not symmetrical along its chord line. Thus, the C_L and C_D are not similar to those of the baseline airfoil. The lift coefficient of the slotted airfoil is slightly negative due to the decrease in pressure on the pressure side of the airfoil as a result of slot flow.

Fig. 10 shows the comparison of the velocity contours of the slotted airfoil and the baseline airfoil for AoA = 12°, 14°,16°, 18°, and 20°. Flow separation starts for the baseline airfoil at AoA = 12° while it is still attached for the slotted airfoil. At AoA = 16°, separation develops further on the suction side of the baseline airfoil while it hardly starts for the slotted airfoil. The same behavior can be observed for AoA = 20° where separation covers nearly 75% of the suction side of the baseline airfoil while the flow remains to be attached on the slotted airfoil. The slot appears to inject efficiently high speed jet on the suction side at all angles of attack. This is clear as the flow velocity adjacent to the slot outlet is high. This behavior consistently prevents flow separation and thus contributes to higher lift coefficient for the slotted airfoil for AoA > 12° and eliminates the stall experienced by the baseline airfoil.

Fig. 11 shows the corresponding pressure coefficient distribution on the pressure and suction sides of both slotted and baseline airfoils. The pressure coefficient is defined:

$$P_c = \frac{P - P_\infty}{\frac{1}{2}\rho V_\infty^2} \quad (1)$$

The baseline airfoil results at AoA = 12° and 16° show smooth pressure recovery on the suction side of the airfoil. At AoA = 20°, however, the pressure remains constant after X/C = 0.5. For the slotted airfoil, on the other hand, the pressure variation on the suction side shows two distinct peaks; one after the leading edge and another after the slot. The negative pressure associated with the secondary peak becomes lower as the angle of attack increases which maintains higher lift coefficient at AoA = 20°. It is important to mention that the slotted airfoil is represented in two separate curves, where it is physically

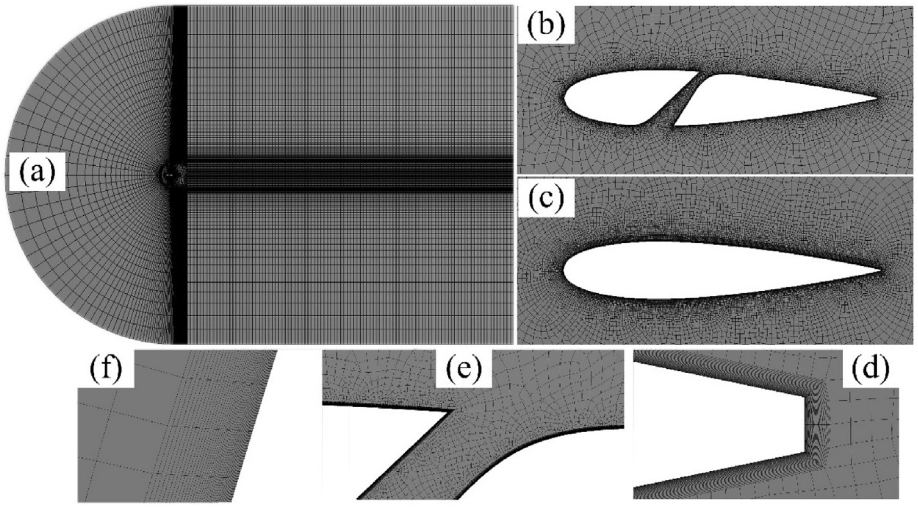

Fig. 4. Airfoil mesh details: (a) full domain; (b) slotted airfoil; (c) baseline airfoil; (d) trailing edge; (e) slot outlet; (f) inflation layers.

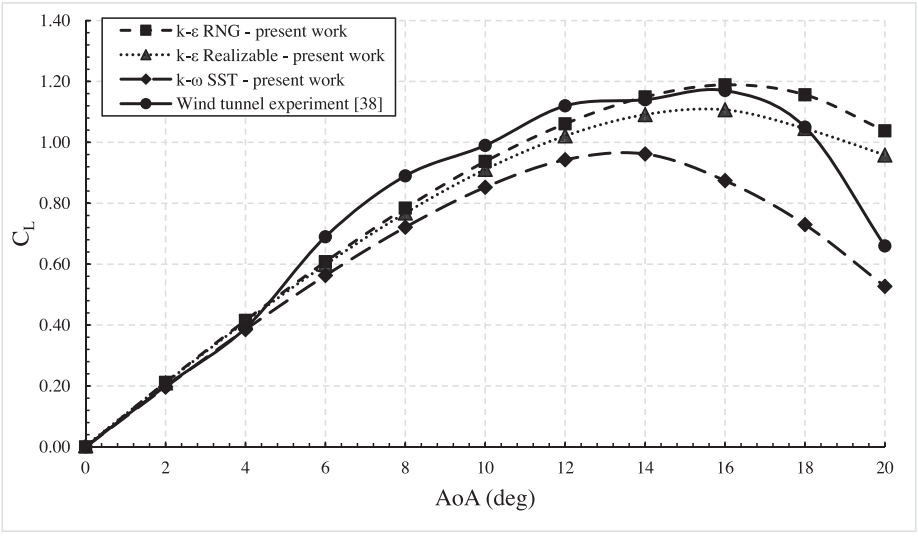

Fig. 5. Predicted lift coefficient for baseline airfoil (NACA0018) – Turbulence model validation.

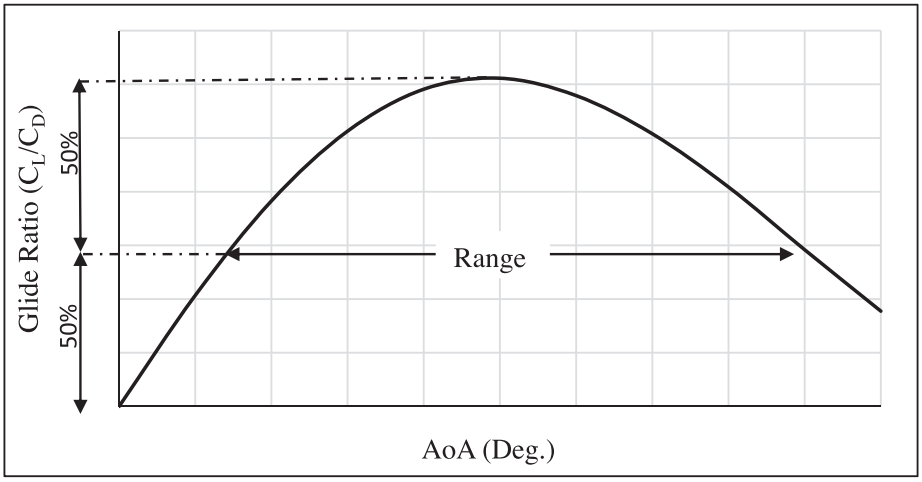

Fig. 6. Descriptive illustration for the slotted airfoil performance evaluation parameters.

Table 4
Slotted airfoil results.

Case #	Maximum glide ratio	AoA range of ½ maximum glide (°)		Range (°)
		From	To	
1	28.88	5	25	20
2	28.73	6	25	19
3	27.76	5	22	17
4	28.32	5	19	14
5	26.57	5	23	18
6	29.18	5	25	20
7	28.19	5	25	20
8	28.44	6	25	19
9	28.8	6	26	20
10	26.87	5	21	16
Baseline	30.56	3	17	14

composed from two parts. As can be seen, at 0.25 < X/C < 0.3 an overlap between the two curves exists, where at this position, both the upper and lower surfaces of the slot are coincident.

5. Application of slotted airfoil in Darrieus-type VAWT

Based on the above investigation of the slotted airfoil and the shown superior behavior, compared with the baseline airfoil in terms of glide ratio range, the selected slotted airfoil configuration 9 was applied to the H-type Darrieus VAWT. Fig. 12 shows the basic 2-dimensional model geometry of 3-bladed Darrieus type VAWT. The blades are arranged on a circle of radius R and rotate with a rotational speed ω. Being exposed to wind of a velocity V_∞, the wind generates aerodynamic forces which result in turbine rotation. The force component which has the major contribution to blade motion is the lift force. Since the angle of attack between the relative wind velocity and the airfoil chord line changes continuously as the blade rotates, the driving forces also change with azimuth angle of the blade θ.

Five dimensionless parameters are used to fully describe the performance of Darrieus type turbine. These are: the moment coefficient (C_m), the power coefficient (C_p), the tip speed ratio (TSR or λ), the Reynold's number (R_e), and the rotor solidity (σ). These parameters are formulated mathematically as follows:

$$C_m = \frac{T}{\frac{1}{2}\rho V_\infty{}^2 AR} \tag{2}$$

$$C_P = \frac{T\omega}{\frac{1}{2}\rho V_\infty{}^3 A} \tag{3}$$

$$\lambda = \frac{\omega R}{V_\infty} \tag{4}$$

$$Re = \frac{\rho V_\infty D}{\mu} \tag{5}$$

$$\sigma = \frac{nC}{D} \tag{6}$$

From Eqs. (2) and (4), the power coefficient (C_P) could be written:

$$C_P = C_m . \lambda \tag{7}$$

Experimental and numerical investigations of VAWT are concerned with obtaining the functional relation between moment coefficient and power coefficient with turbine's tip speed ratio, Reynolds number and solidity ratio.

The angle of attack for each blade, the angle between the blade chord and the direction of relative wind velocity, can be calculated based on the direction of the relative velocity and blade azimuth position. The relative wind velocity is the vector difference between the blade velocity ($\vec{\omega R}$) and wind velocity $\vec{V\infty}$:

$$\vec{V_r} = \vec{V_\infty} - \vec{\omega R} \tag{8}$$

Using the relationship between azimuth position (θ) and relative velocity direction, the equation describing the variation of the angle of attack (AoA) with azimuth position can be written (see Fig. 12):

$$AoA = \tan^{-1}\left(\frac{\sin\theta}{\lambda + \cos\theta}\right) \tag{9}$$

Based on equation (9), the theoretical AoA could be calculated at each azimuth position for different TSR, Fig. 13. Based on these theoretical values, the working range of AoA is inversely proportional to the TSR. At TSR = 2 the working range of AoA is between +30° and −30°. However, this range is reduced by 20° at TSR = 3. at TSR = 3 the working range of AoA is between +20° and −20°. Therefore, the slotted airfoil behavior is expected to outperform the baseline airfoil at low TSR, where the working range of AoA is high.

The turbine simulations were performed using the computational domain shown in Fig. 14. The domain dimensions were verified by Balduzzi et al. [39]. The domain extends 30D on both sides of the turbine centerline, where D is the turbine diameter. The selected upstream domain length is 40D while the downstream length is 100D. These dimensions ensure domain independent solution.

The domain is divided into two subdomains utilizing the sliding mesh technique, where a stationary domain is rectangular in shape, and a rotating zone where the turbine is laid is circular. The rotating zone diameter is 2 times the diameter of the turbine. The mesh details were adopted from [40].

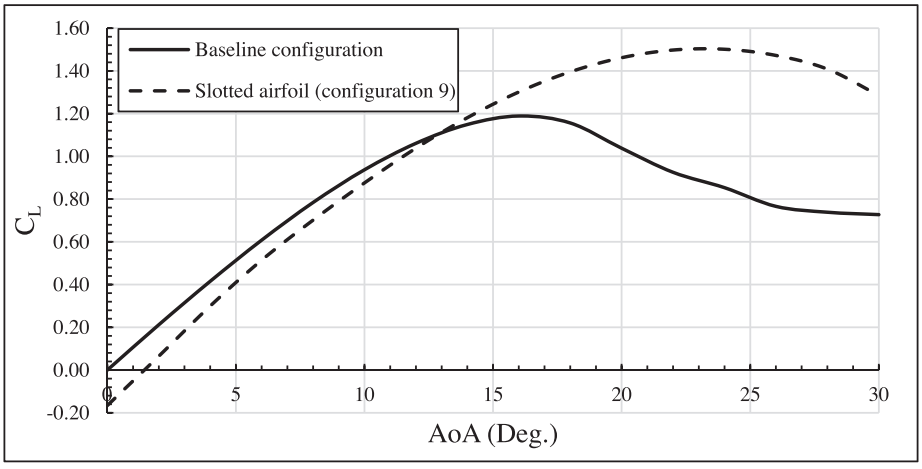

Fig. 7. Predicted variation of lift coefficient with angle of attack for selected slotted airfoil and baseline airfoil.

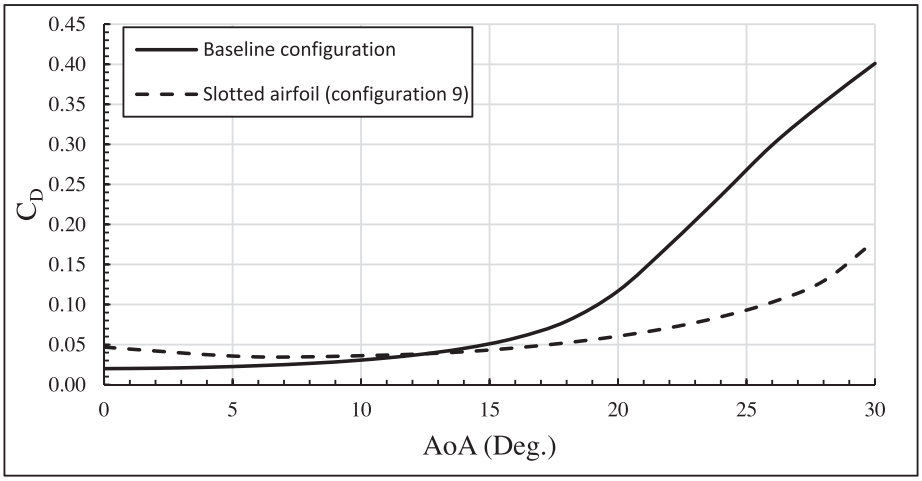

Fig. 8. Predicted variation of drag coefficient with angle of attack for selected slotted airfoil and baseline airfoil.

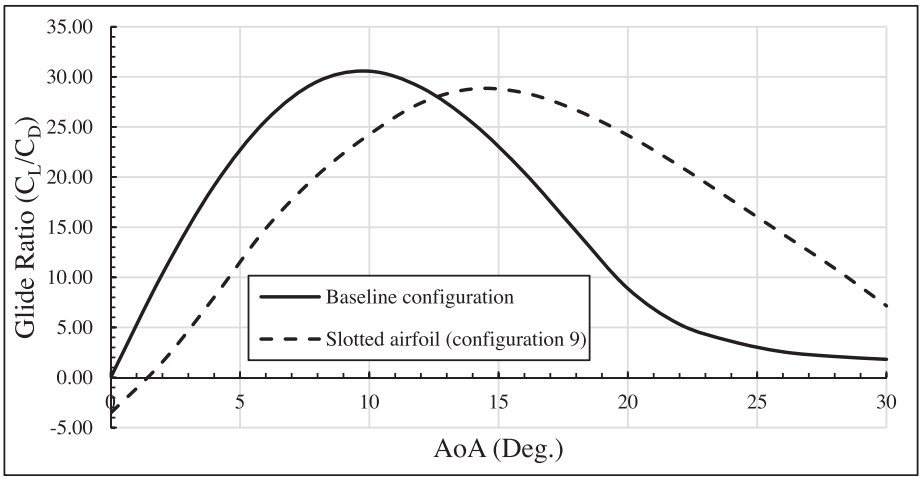

Fig. 9. Predicted variation of glide ratio with angle of attack of the selected slotted airfoil and baseline airfoil.

A mesh of approximately 400,000 nodes was created for turbine simulations at which 40 inflation layers, with proper first layer thickness, were created on the airfoils' walls to maintain a y^+ value less than one. Fig. 15 shows details of the numerical mesh used for the 3 bladed turbine. Coupled algorithm was utilized to solve the momentum and pressure-based continuity equations together with second order upwind discretization for all Unsteady Reynolds Averaged Navier-Stokes equations (URANS) and turbulence equations. The convergence residuals were all set to be 10^{-5} using a step size of 0.5° for all turbine simulations. Second order implicit time discretization scheme was adopted. The flow equations were solved using ANSYS-FLUENT 16 [41]. The realizable k-ε turbulence model was used in all turbine simulations.

Turbine dimensions used in the present simulations are shown in table 5. The turbine diameter is 4.7 m where the chord length of each blade is 0.47 m. The corresponding solidity of the turbine is 0.3 where the turbine is expected to operate optimally at low TSR [42,43]. Two types of NACA 0018 airfoil were employed; the baseline airfoil (BL) and the slotted airfoil (SA) (configuration 9).

6. Results of the turbine simulations

The turbine simulations were performed using a fixed wind speed of 8 m/s. The rotational speed of the turbine was varied to obtain the required TSR. Fig. 16 shows the predicted variation of the turbine torque coefficient with tip speed ratio for both the slotted airfoil (SA) turbine and the baseline (BL) turbine. The TSR was varied between 1 and 3.5. As can be seen, a significant increase of the torque coefficient is achieved by the SA turbine, compared to the BL turbine, at low TSR. The turbine behavior at low TSR affects the starting characteristics of the turbine. The BL turbine has a very low torque at low TSR. On the other hand, the SA turbine performance declines at high TSR (> 2.5), where the working range of AoAs at higher TSR decreases where the SA blade has lower performance compared with BL blade at low AoA. The SA turbine has a maximum torque coefficient of 0.15 at TSR = 2, which is more than double that of the BL turbine at the same TSR. On the other hand, the peak torque coefficient of the BL turbine is 0.118 observed at TSR = 2.5.

In order to understand the reason for high turbine torque at TSR = 1 produced by the SA turbine, the variation of the instantaneous torque coefficient with the azimuth position for a single blade is examined in Fig. 17. The torque coefficient has been significantly enhanced at this TSR thanks to the optimized slotted airfoil. As can be noticed in Fig. 18, the peak torque coefficient at $\theta = 50^\circ - 60^\circ$ is nearly 50% higher for the SA turbine. Also, continuous fluctuations of torque are observed for the BL turbine just after the peak torque. These fluctuations in torque can be inferring the presence of vortex shedding, which occurs in the rotating flow field because of the interactions between the wind and the blades. It is important to mention that the vortex shedding phenomenon strongly affects the extraction of energy in VAWTs, as it decreases the instantaneous torque to become negative value at $150^\circ < \theta < 360^\circ$. Furthermore, at the same TSR, the proposed

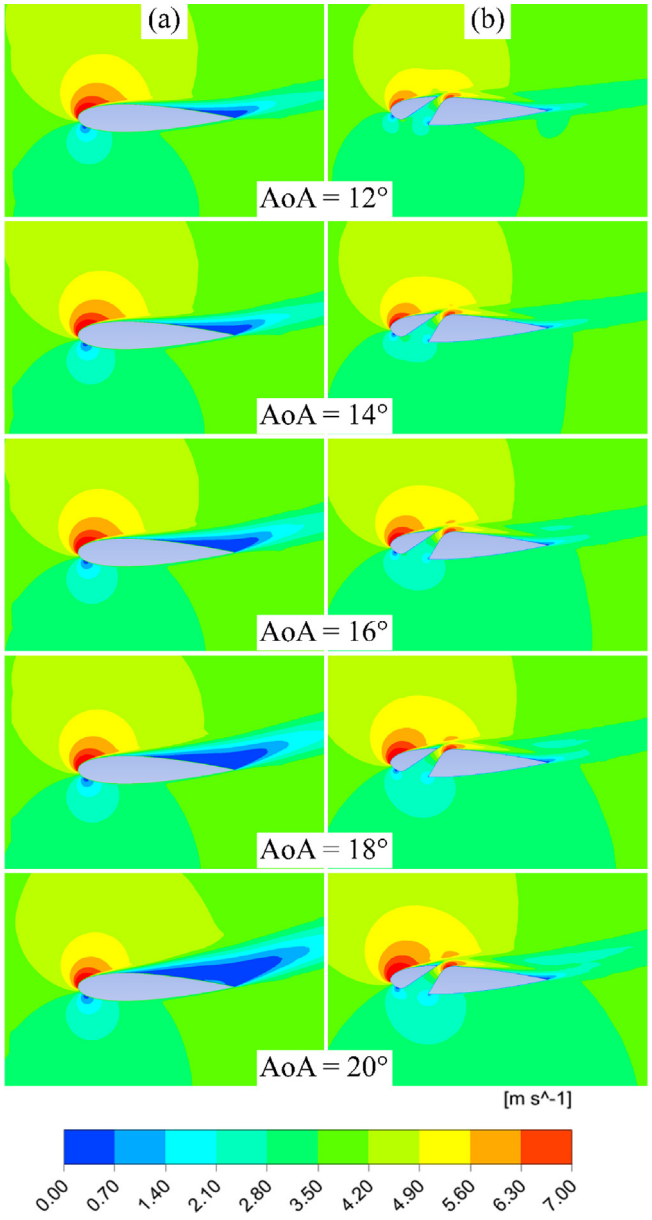

Fig. 10. Comparison between velocity contours for (a) case 9 slotted airfoil and (b) baseline airfoil at AoA = 12°, 16°, and 20°.

SA turbine is resulting in less fluctuations as can be seen from Fig. 17, which eliminates partially the presence of negative torque.

In Fig. 18, the computed variation of the torque coefficient relative to azimuth position (θ) is plotted for TSR = 2. As can be noticed, the peak toque is almost occurring at the same azimuth position for both turbines. However, the BL turbine is still having a significant torque degradation when the blade is on the downwind position ($150^\circ < \theta < 360^\circ$), where the frequent oscillations of the torque coefficient are still present, though, the negative torque has slightly decreased. On the other hand, the torque variation for the SA turbine is similar to the trend at TSR = 1, however, the peak positive torque takes wider range of azimuth positions. Consequently, the average torque coefficient of SA turbine at this TSR is the highest approaching a value of 0.15 compared to 0.055 for the BL turbine. The SA turbine negative torque is small, and its instantaneous peak torque is significantly higher than the BL turbine.

Moving to TSR = 2.5, the average torque coefficient for both SA turbine and BL turbine are very close; the average torque coefficient for

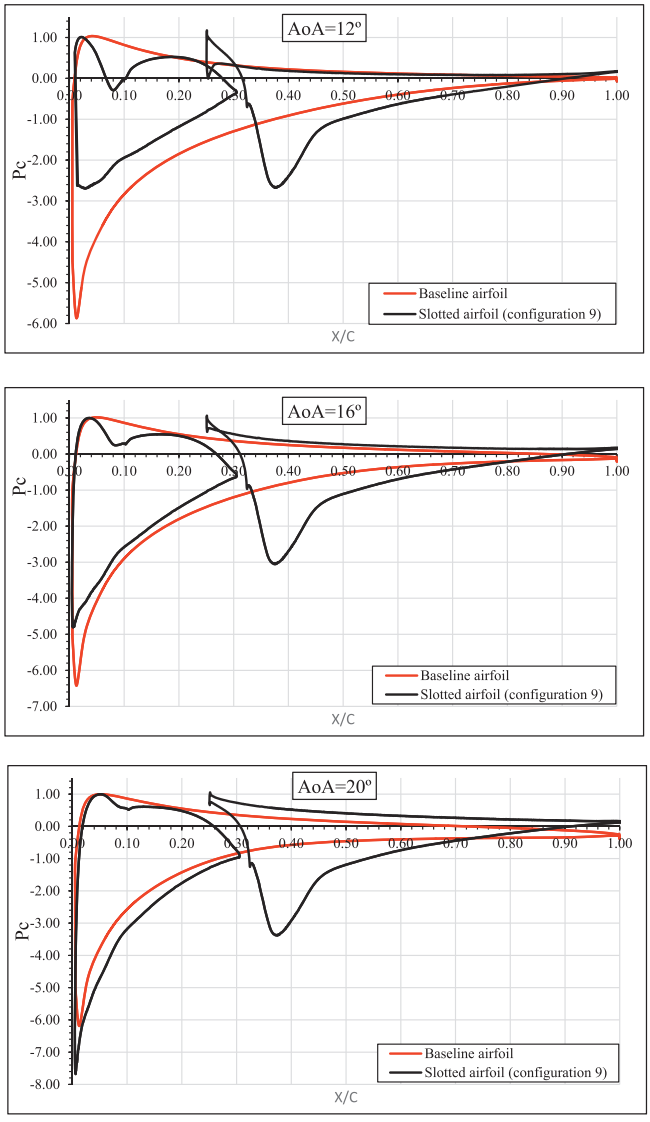

Fig. 11. Comparison between pressure coefficients on suction and pressure sides for both slotted airfoil (configuration 9) and baseline airfoil at AoA = 12°, 16°, and 20°.

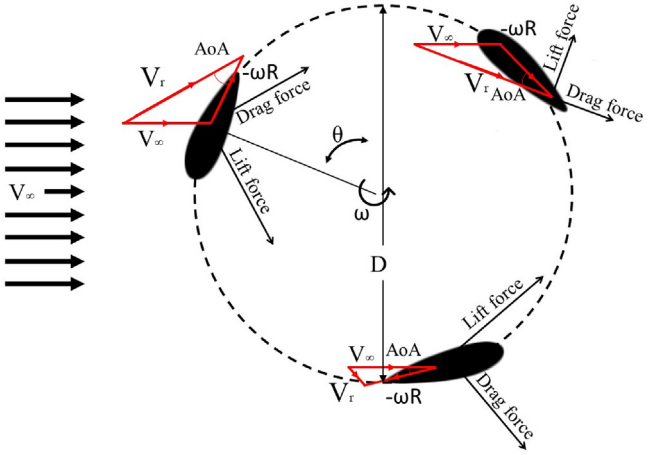

Fig. 12. Geometry and parameters of the Darrieus rotor and force analysis.

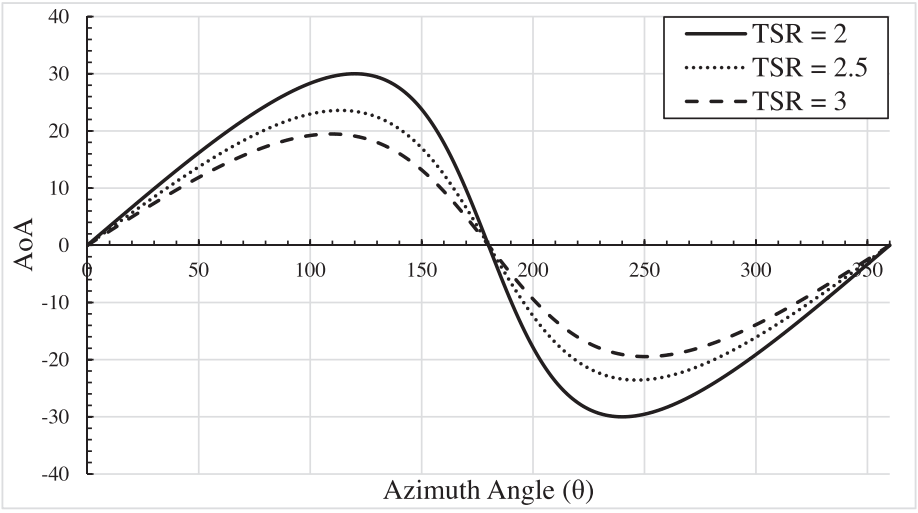

Fig. 13. Theoretical AoA variation with azimuth position for different TSR.

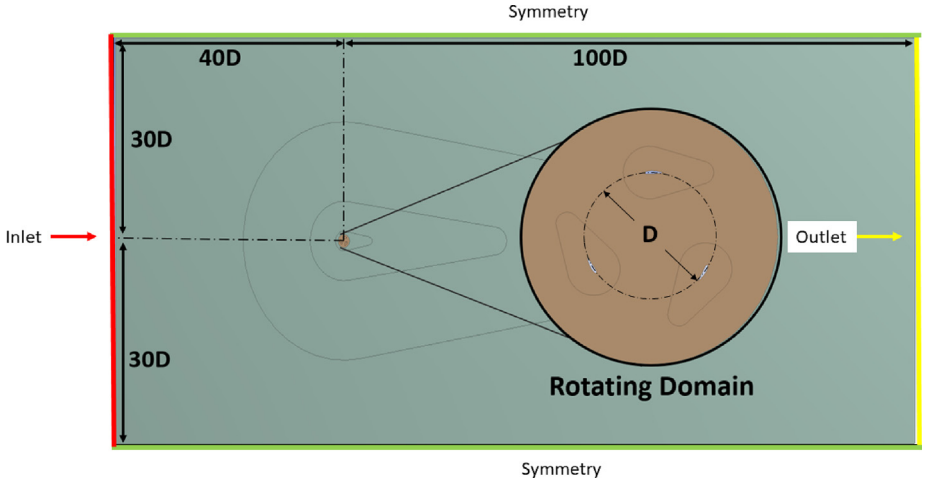

Fig. 14. Dimensions of the turbine computational domain.

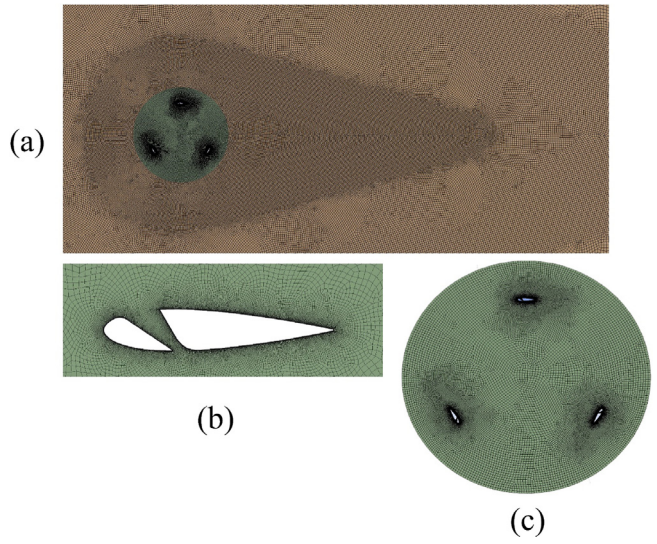

Fig. 15. Mesh details for SA turbine: (a) overall domain: (b) airfoil; (c) rotating domain.

Table 5
Turbine geometry used in the present study.

Number of Blades	3
Blade type	NACA 0018/BL and SA
Rotor Diameter (D) [m]	4.7
Blade chord length (C) [m]	0.47
Solidity (σ)	0.3

SA turbine and BL turbine are 0.102 and 0.118, respectively. Nonetheless, the variation of torque along a full revolution cycle as shown in Fig. 19 does not follow the same trend for both turbines. At this TSR, the SA turbine is characterized by higher peak torque coefficient as well as wide range of negative torque which extends within $0^{\circ} < \theta < 30^{\circ}$ and $165^{\circ} < \theta < 360^{\circ}$. The presence of negative torque is the main reason behind the degradation in average torque coefficient of the SA turbine at high TSR. For the BL turbine, at the same TSR, it is shown that the negative torque has been eliminated partially compared to smaller TSR, which causes significant improvement to its average torque coefficient.

Fig. 20 shows the predicted variation of the torque coefficient for one complete revolution at TSR = 3, where the BL turbine is having an average torque coefficient of 0.117, while the average torque coefficient of SA turbine is 0.062. Nevertheless, the slotted airfoil turbine is still having a higher peak instantaneous torque compared with the BL

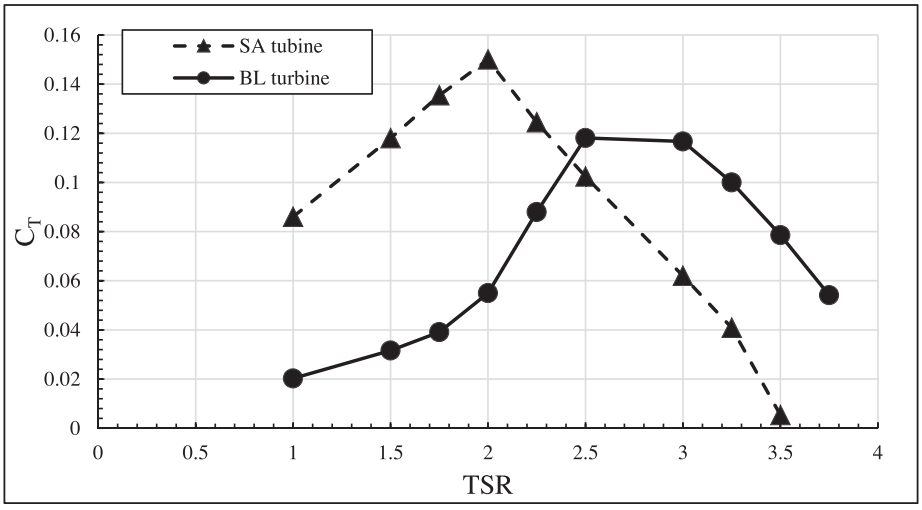

Fig. 16. Variation of torque coefficient along different tip speed ratios for the SA turbine and BL turbine.

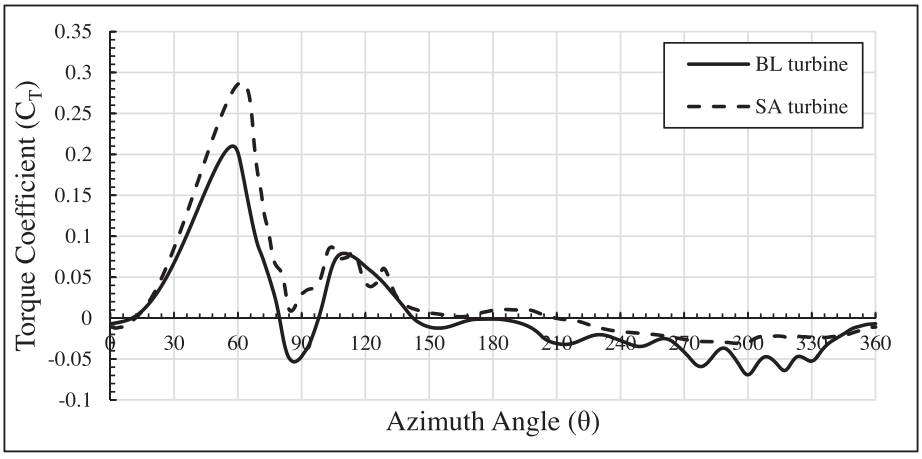

Fig. 17. Variation of the torque coefficient with the azimuth angle for one blade at TSR 1.

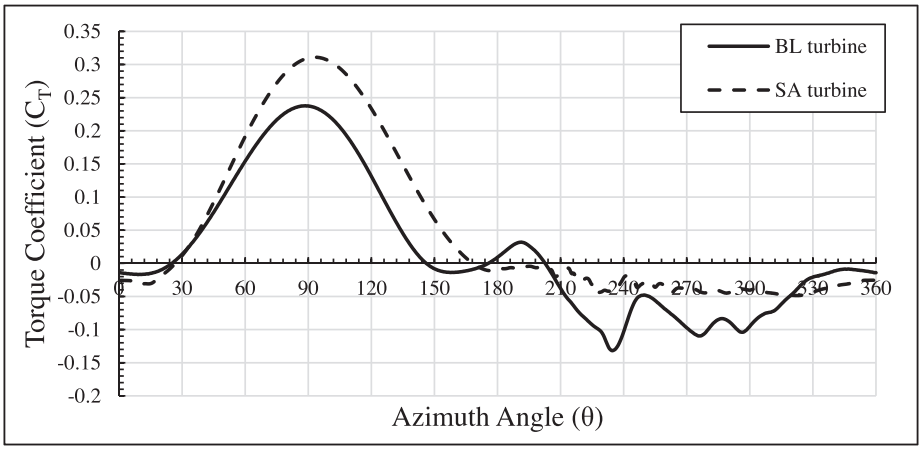

Fig. 18. Variation of the torque coefficient with the azimuth angle for one blade at TSR 2.

turbine. Furthermore, degradation in torque can be noticed when $0^\circ < \theta < 40^\circ$ and $160^\circ < \theta < 360^\circ$. On the other hand, the BL turbine torque profile is having a smaller peak compared to the SA turbine, however, a significant enhancement in average torque coefficient of BL turbine could be noticed, where the negative torque is partially eliminated and another small peak is present at $190^\circ < \theta < 340^\circ$, which is the reason behind this increase in overall torque coefficient of the BL turbine. The negative torque noticed in the predictions of the SA turbine during the downstream part of the cycle can be attributed to the bad performance of the SA at negative angles of attack where the pressure side of the airfoil coincides with the outlet side of the slot. The opposite effect happens on the inlet side of the slot where it coincides with the suction side of the airfoil. The reversed positions reduces the lift force of the airfoil and causes negative torque contribution at this

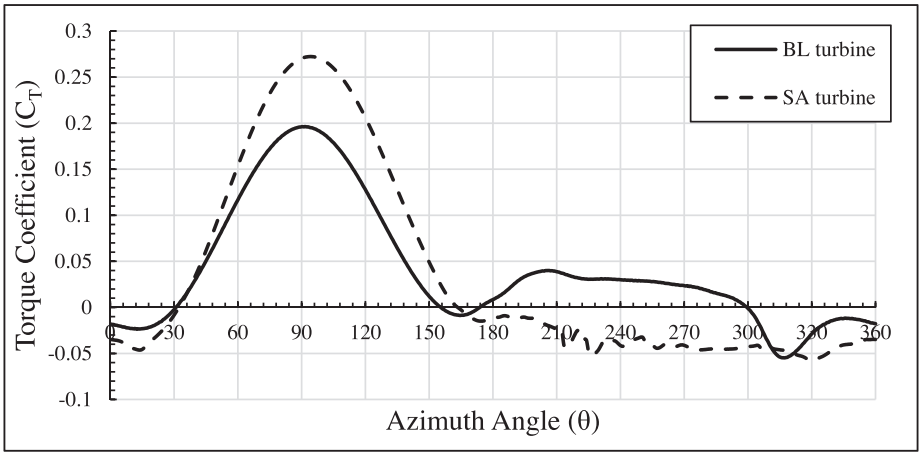

Fig. 19. Variation of the torque coefficient with the azimuth angle for one blade at TSR 2.5.

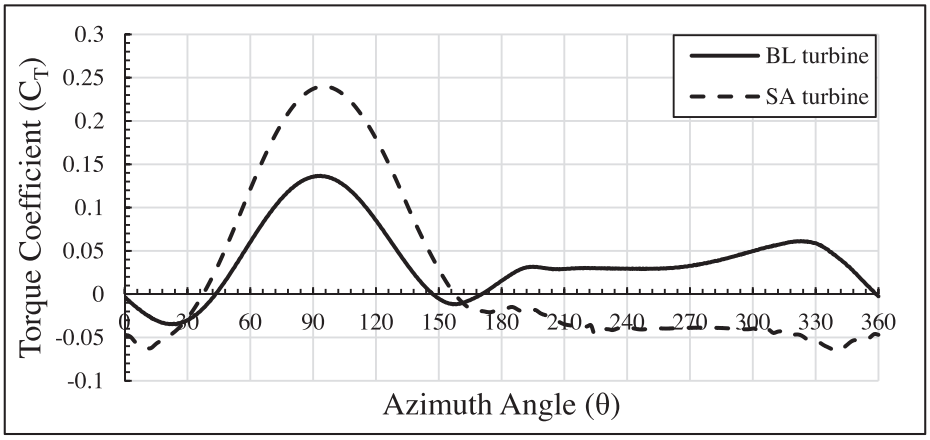

Fig. 20. Variation of the torque coefficient with the azimuth angle for one blade at TSR 3.

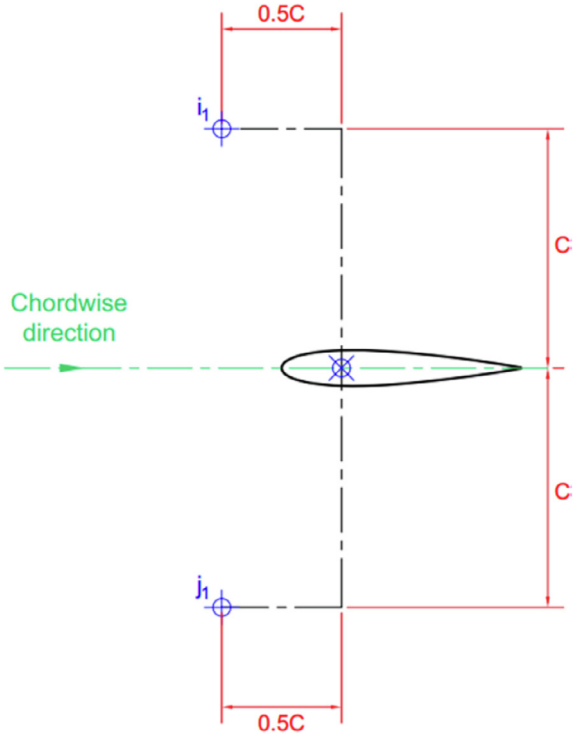

Fig. 21. Reference points to calculate magnitude and direction of freestream wind velocity [44].

Table 6
Values of AoA and corresponding C_L at θ_{max} for TSR = 1, 2, 2.5 and 3.

Turbine type	BL	SA	BL	SA	BL	SA	BL	SA
Peak C_T	0.186	0.29	0.235	0.311	0.195	0.272	0.136	0.24
TSR	1		2		2.5		3	
θ_{max}	61.5°		93°		94.5°		95.5°	
AoA_{th}	30.8°		27.1°		22.4°		18.9°	
AoA_{actual}	32.6°	34.6°	25.8°	27.7°	19.6°	21.1°	14.3°	16.6°
$C_{L\ actual}$	0.717	1.002	0.777	1.417	1.067	1.482	1.156	1.334

TSR during the downstream part of the blade cycle.

Previous analysis showed that the peak positive torque coefficient for the SA turbine is always higher than that of the BL turbine when they operate at the same TSR. Further analysis is carried out for BL and SA turbines at the same azimuth position where the maximum torque coefficient is occurring (θ_{max}). In this analysis the actual angle of attack is computed adopting the methodology carried out by Elsaka et al. [44], where a reference points was taken at positions i_1 and j_1 as shown in Fig. 21. The magnitude and direction of the wind velocity are computed from the CFD results. Using this method, the actual angle of attack acting on the blade (AoA_{actual}) could be calculated. Table 6 shows the concluded angles of attack at θ_{max} at different TSRs. Table 6 also includes the theoretical angle of attack AoA_{th} calculated using equation (9) for each TSR. For each angle of attack the corresponding lift coefficient C_L is indicated based on the results obtained in the present study (section 4 above). As can be seen, the C_L for SA turbine is always higher compared to the BL turbine blade, at θ_{max} thanks to the delay in flow separation which allows the blade to have high lift force at high AoA.

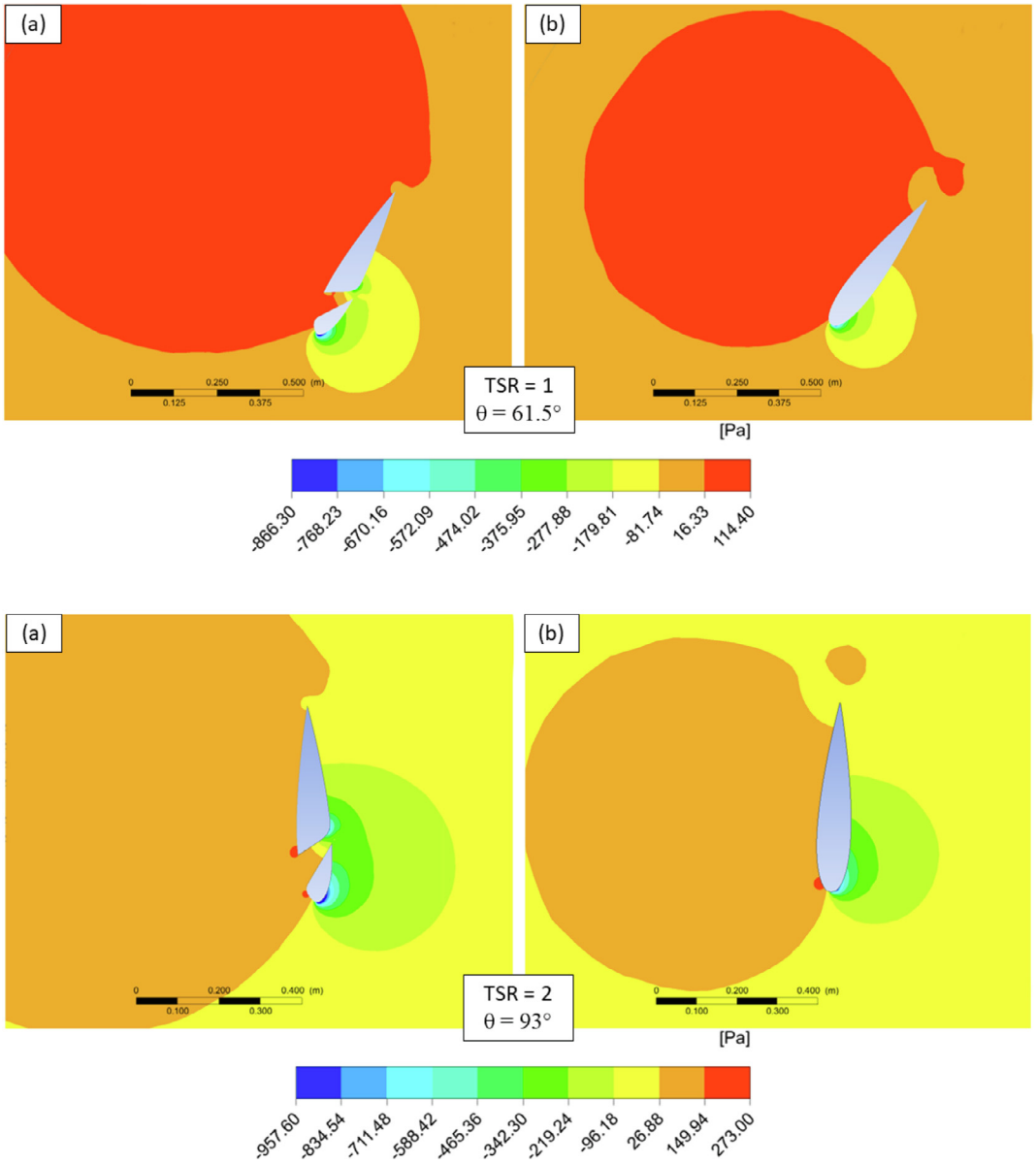

Fig. 22. Static pressure contours for (a) SA and (b) BL turbines for one blade at the position of maximum torque.

This justifies the higher peak torque coefficient for SA turbine.

Further examination of the pressure field for both BL and SA turbines at θ_{max} for each TSR can be found in Fig. 22. As can be noticed, at the pressure side the SA is having a higher positive pressure for all TSR causing the higher lift force as discussed earlier. It is also observable that at TSR = 2, 2.5, and 3, the SA turbine blade has two peak negative pressure points compared to one point for BL airfoil. Zones covered by negative pressure on the suction side of the SA are also wider, indicating no separation. The negative pressure at the slot outlet is another indication on the jet flow out of the slot at all values of the TSR. It is also of interest to note that the first part of the slotted airfoil adds extra lift force producing area to the overall airfoil.

Fig. 23 shows the predicted variation of the average power coefficient at different TSR for both the SA and the BL turbines. The figure shows that the power coefficient of the SA turbine is significantly higher than that of the BL at low TSR. However, this trend is reversed at high TSR. The peak power coefficient of the SA turbine is 0.3 and occurs at TSR = 2, while that of the BL turbine is 0.35 and occurs at TSR = 3.

7. Static simulations results

In order to examine the starting characteristics of the Darrieus turbine using SA, simulations were performed without turbine rotation; i. e. steady state simulations. The aerodynamic torque on the 3 bladed rotor was computed at different rotor azimuth angles which simulates starting conditions of the turbine. The azimuth angle of the rotor was changed in 10° steps. At each position, steady state simulations were carried out.

Fig. 24 shows the computed torque coefficient for fixed turbine at different azimuth positions of the rotor. The results show that both the SA and the BL turbines has negative torque for small azimuth angles. As the azimuth angle increases, the static torque increases and the SA turbine shows much higher torque. The static torque decreases again and reaches negative values at an azimuth position of 120°. This pattern is repeated again through further increase of the azimuth angle since the turbine is 3 bladed. The maximum static torque of the SA turbine and the BL turbine occurs at approximately 70°. The maximum static torque of the SA turbine is nearly 50% higher than that of the BL turbine. This implies that the slotted airfoil could be used to enhance the

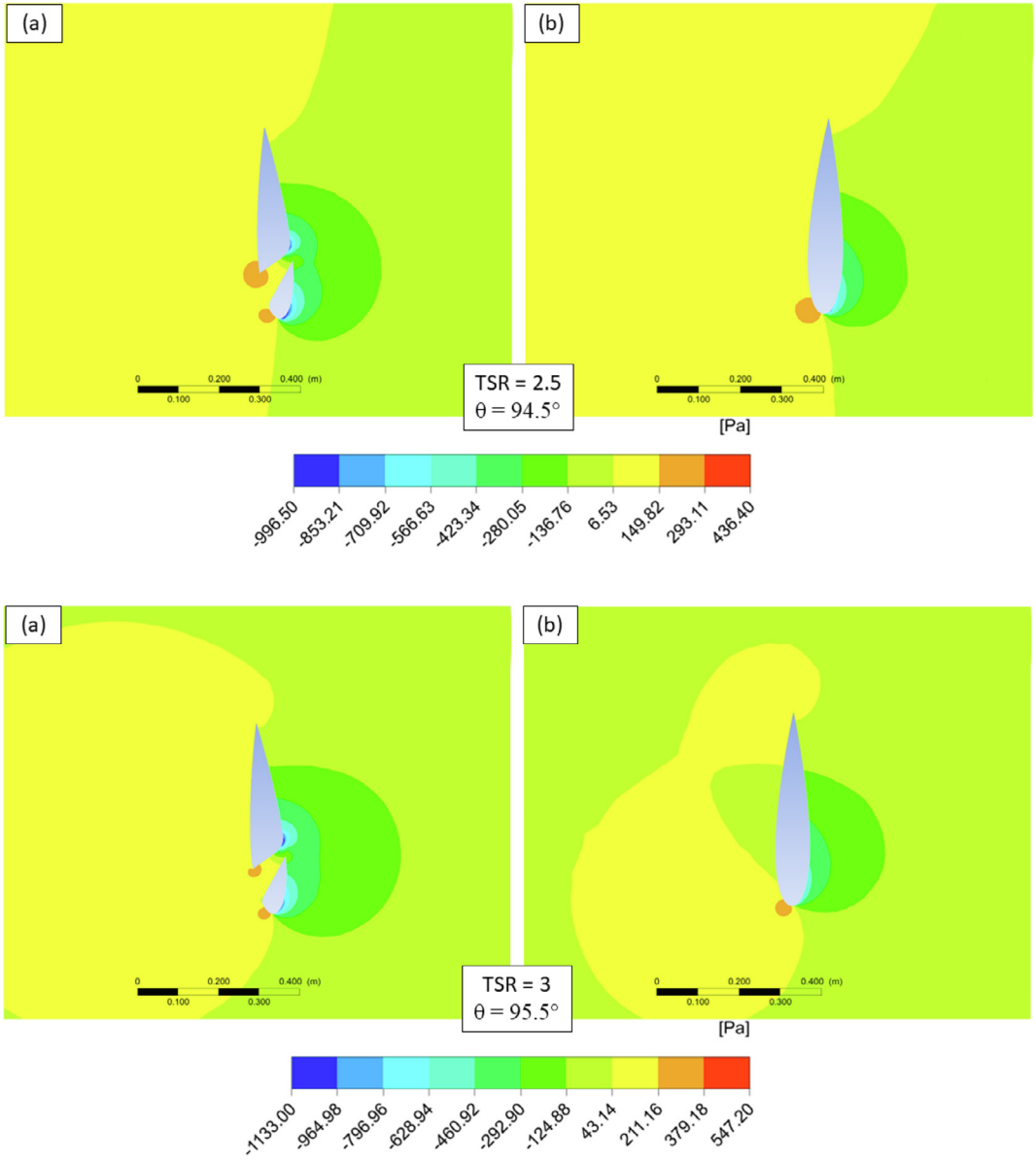

Fig. 22. (*continued*)

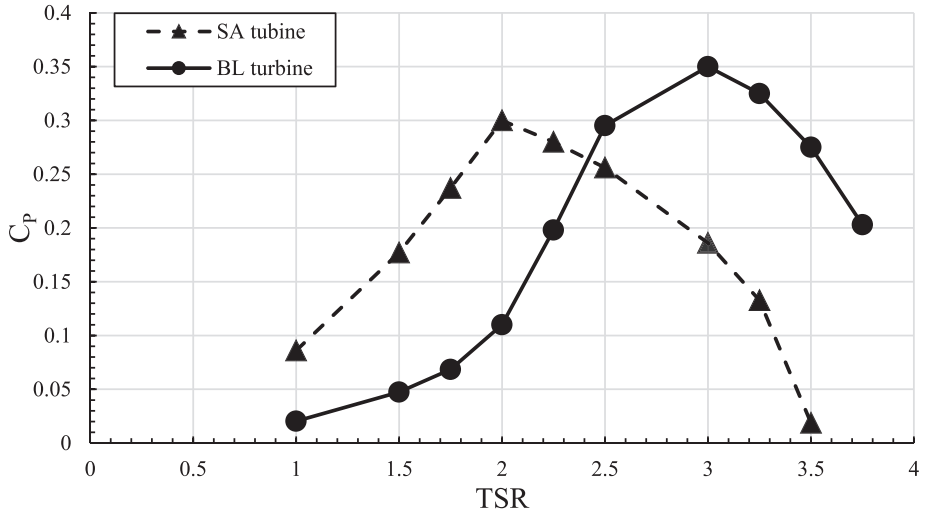

Fig. 23. Variation of power coefficient with TSRs for the proposed SA turbine and conventional BL turbine.

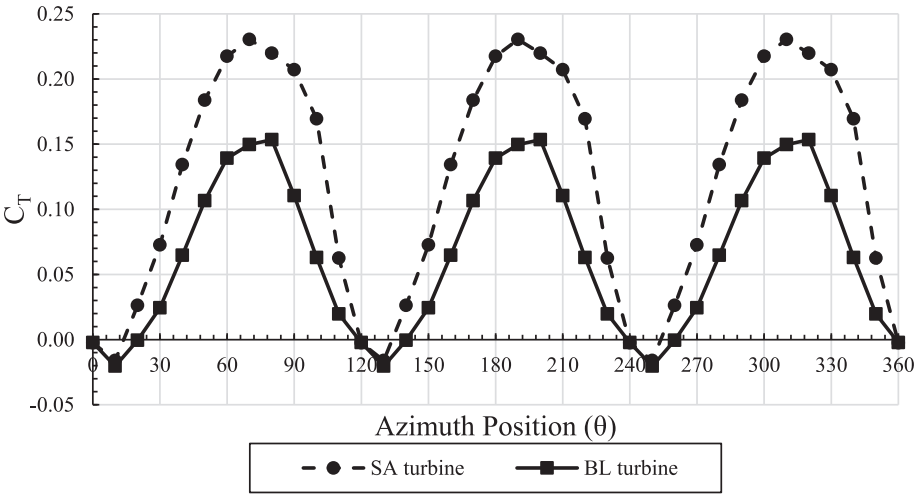

Fig. 24. Variation in torque coefficient at zero angular velocity for SA and BL turbines and different.

starting torque of VAWTs.

8. Conclusion

The present investigation has highlighted the advantages of using slotted airfoil blade in Darrieus type VAWT. The performance of slotted airfoil turbine was examined using CFD tools. Initially, the slot concept was applied to static NACA0018 airfoil at different angles of attack to verify its advantages on flow separation at high angles of attack. Thus, the slot geometrical parameters were optimized based on static behavior results. Thereafter, the selected slotted airfoil configuration was applied to the Darrieus rotor. The effect of the slot was investigated from different perspectives. The major findings of the present work can be summarized as follows:

- The slotted airfoil effectively delays the boundary layer separation, where at high angles of attack the slot allows part of high pressure flow to pass into the suction side of the airfoil causing an acceleration in the flow due to the nozzle shape of the slot. Consequently, this minimizes the drag force and increases the lift force at high angles of attack. Hence, the slotted airfoil achieves similar glide ratio to baseline airfoil; however, the peak glide ratio covers wider range of angles of attack while using the slotted airfoil.
- The application of slotted airfoil blade to Darrieus type turbine significantly augments both the torque coefficient and the power coefficient at low TSR, while at high TSR the power coefficient of SA turbine notably decreases.
- The SA turbine has a maximum torque coefficient of 0.15 at TSR = 2, which is approximately 3 times that of the BL turbine at the same TSR.
- At TSR = 2 the SA turbine calculated power coefficient is 0.3 which is approximately 3 times that of the BL turbine at the same TSR. However, at TSR = 3 the SA turbine computed power coefficient is 0.19 which is 54% of that of the BL turbine.
- It can be concluded that the self-starting capability of SA turbine is far better that of BL turbine. While the rotor is at rest with no rotation, the SA turbine shows higher torque coefficient at all azimuth positions.

Finally, it is important to mention that future works, which aim to focus on wind tunnel experimental study of slotted airfoil Darrieus type turbine, will need to be undertaken.

Declaration of Competing Interest

The authors declare that they have no known competing financial interests or personal relationships that could have appeared to influence the work reported in this paper.

References

[1] Tjiu W, Marnoto T, Mat S, Ruslan MH, Sopian K. Darrieus vertical axis wind turbine for power generation I: Assessment of Darrieus VAWT configurations. Renewable Energy 2015;75:50–67.
[2] Borg M, Shires A, Collu M. Offshore floating vertical axis wind turbines, dynamics modelling state of the art. part I: aerodynamics. Renew Sustain Energy Rev 2014;39:1214–25.
[3] Kumar R, Raahemifar K, Fung AS. A critical review of vertical axis wind turbines for urban applications. Renew Sustain Energy Rev 2018;89:281–91.
[4] Hosseini A, Goudarzi N. Design and CFD study of a hybrid vertical-axis wind turbine by employing a combined Bach-type and H-Darrieus rotor systems. Energy Convers Manage 2019;189:49–59.
[5] S. Fertahi, T. Bouhal, O. Rajad, T. Kouskou, A. Arid, T. Rhafiki, A. Jamil, A. Benbassou, "CFD performance enhancement of a low cut-in speed current Vertical Tidal Turbine through the nested hybridization of Savonius and Darrieus" Journal of Energy Resources Technology, vol. 142, 2020.
[6] Roshan A, Sagharichi A, Maghrebi MJ. Nondimensional parameters' effects on hybrid darrieus-savonius wind turbine performance. Energy Conversation Manage 2018;169:266–78.
[7] Tian W, Yang Z, Zhang Q, Wang J, Li M, Ma Y, et al. Bionic design of wind turbine blade based on long-eared owl's airfoil. Appl Bionics Biomech 2017.
[8] Sengupta AR, Biswas A, Gupta R. Studies of some high solidity symmetrical and unsymmetrical blade H-Darrieus rotors with respect to starting characteristics, dynamic performances and flow physics in low wind streams. Renewable Energy 2016;93:536–47. https://doi.org/10.1016/j.renene.2016.03.029.
[9] Scungio M, Arpino F, Focanti V, Profili M, Rotondi M. Wind tunnel testing of scaled models of a newly developed Darrieus-style vertical axis wind turbine with auxiliary straight blades. Energy Convers Manage 2016;130:60–70. https://doi.org/10.1016/j.enconman.2016.10.033.
[10] Bai Y, Ma X, Ming X. Lift enhancement of airfoil and tip flow control for wind turbine. Appl Math Mech 2011;32:825–36.
[11] Al-Shohani M. Numerical Analysis of a Modified Airfoil for Wind Turbine. Diyala J Eng Sci 2014;07(02):38–79.
[12] Wang H, Jiang X, Chao Y, Li Q, Li M, Zheng W, et al. Effects of leading edge slat on flow separation and aerodynamic performance of wind turbine. Energy 2019;182:988–98.
[13] Wong K, Chong W, Sukiman N, Shiah Y, Chew S, Sopian K, et al. Experimental and simulation investigation into the effects of a flat plate deflector on vertical axis wind turbine. Energy Convers Manage 2018;160:109–25.
[14] Lee Y, Zhao S, Tagawa K, Feng F. Starting performance effect of a truncated-cone shaped wind gathering device on small-scale straight-bladed vertical axis wind turbine. Energy Convers Manage 2018;167:70–80.
[15] Patel V, Eldho TI, Prabhu SV. Experimental investigations on darrieus straight blade turbine for tidal current application and parametric optimization for hydro farm arrangement. Int J Mar Energy 2017;17:110–35.
[16] Patel V, Eldho TI, Prabhu SV. Performance enhancement of a Darrieus hydrokinetic turbine with the blocking of a specific flow region for optimum use of hydropower. Renewable Energy 2019;135:1144–56.
[17] Lositaño I, Danao L. Steady wind performance of a 5 kW three-bladed H-rotor Darrieus Vertical Axis Wind Turbine (VAWT) with cambered tubercle leading edge

(TLE) blades. Energy 2019;175:278–91.
[18] Wang Z, Zhuang M. Leading-edge serrations for performance improvement on a vertical-axis wind turbine at low tip-speed-ratios. Appl Energy 2017;208:1184–97.
[19] Wang Z, Wang Y, Zhuang M. Improvement of the aerodynamic performance of vertical axis wind turbines with leading-edge serrations and helical blades using CFD and Taguchi method. Energy Conversation Manage 2018;177:107–21.
[20] Sobhani E, Ghaffari M, Maghrebi MJ. Numerical investigation of dimple effects on darrieus vertical axis wind turbine. Energy 2017;133:231–41.
[21] Zhu H, Hao W, Li C, Ding Q. Numerical study of effect of solidity on vertical axis wind turbine with Gurney flap. J Wind Eng Ind Aerodyn 2019;186:17–31.
[22] Shukla V, Kaviti AK. Performance evaluation of profile modifications on straight-bladed vertical axis wind turbine by energy and Spalart Allmaras models. Energy 2017;126:766–95.
[23] Bianchini A, Balduzzi F, Di Rosi D, Ferrera G. On the use of Gurney Flaps for the aerodynamic performance augmentation of Darrieus wind turbines. Energy Convers Manage 2019;184:402–15.
[24] Hao W, Ding Q, Li C. Optimal performance of adaptive flap on flow separation control. Comput Fluids 2019;179:437–48.
[25] Sengupta AR, Biswas A, Gupta R. Comparison of low wind speed aerodynamics of unsymmetrical blade H-Darrieus rotors-blade camber and curvature signatures for performance improvement. Renewable Energy 2019;139:1412–27.
[26] Ma N, Lei H, Han Z, Zhou D, Bao Y, Zhang K, et al. Airfoil optimization to improve power performance of a high-solidity vertical axis wind turbine at a moderate tip speed ratio. Energy 2018;150:236–52.
[27] Zhong J, Lee J, Gue P, Wang Y. Dynamic stall control on a vertical axis wind turbine aerofoil using leading-edge rod. Energy 2019;174:246–60.
[28] Parker HF," Variable Camber Rib for Aeroplane Wings". U.S. Patent No. 1341758 A., 1920.
[29] Weick JA, "The Effect of Multiple Fixed Slots and a Trailing-edge Flap on the Lift and Drag of a Clark Y Airfoil, NACA Report No.427, page 6, 1933.
[30] Ramzi M, Abederrahmane G. Passive control via slotted blading in a compressor cascade at stall condition. J Appl Fluid Mech 2013;6:571–80.
[31] Yeo H, and Lim J. "Application of a slotted airfoil for UH-60A helicopter performance" In: Proceedings of the American Helicopter Society Aerodynamics, Acoustics, and Test and Evaluation Technical Specialist Meeting. San Francisco, CA, 2002.
[32] Narsipur S, Pomeroy B, Selig M, "CFD Analysis of Multielement Airfoils for Wind Turbines", 30th AIAA Applied Aerodynamics Conference, Fluid Dynamics and Co-located Conferences, 2012.
[33] Belamadi R, Djemili A, Ilinca A, Mdouki R. Aerodynamic performance analysis of slotted airfoils for application to wind turbine blades. J Wind Eng Ind Aerodyn 2016;151:79–99.
[34] Jacobes EN, Ward KE, Pinkerton RM, "The Characteristics of 78 Related Airfoil Sections from Tests in The Variable-density Wind Tunnel" National Advisory Committee for Aeronautics, Report No. 460, 1933.
[35] Shih TH, Liou WW, Shabbir A, Yang Z, Zhu J. A New κ – εEddy-viscosity model for high reynolds number turbulent flows – model development and validation. Computers Fluids 1995;24(3):227–38.
[36] Menter FR. Two-equation eddy-viscosity turbulence models for engineering applications. AIAA J 1994;32(8):1598–605.
[37] Orszag SA, Yakhot V, Flannery WS, Boysan F, Choudhury D, Maruzewski J, Patel B. "Renormalization Group Modeling and Turbulence Simulations" International Conference On Near-Wall Turbulent Flows, Tempe, Arizona, 1993.
[38] Eggert CA, Rumsey CL. CFD study of NACA 0018 airfoil with flow control. Hampton, Virginia: National Aeronautics and Space Administration; 2017.
[39] Balduzzi F, Bianchini A, Maleci R, Ferrara G. Critical issues in the CFD simulation of Darrieus wind turbines. Renewable Energy 2016;85:419–35.
[40] Mohamed OS, Ibrahim A, Elbaz AR. CFD investigation of the multiple rotors Darrieus type turbine performance. In: Proceedings of the ASME Turbo Expo 2019: Turbomachinery Technical Conference and Exposition. Oil and Gas Applications; Supercritical CO_2 Power Cycles; Wind Energy, vol. 9; 2019. https://doi.org/10.1115/GT2019-91491 [GT2019-91491, V009T48A010, In this issue].
[41] Inc ANSYS. ANSYS Fluent documentation: User guide. ANSYS Inc, Canonsburg, PA: Technical report; 2016.
[42] Eboibi O, Danao LM, Howell RJ. Experimental investigation of the influence of solidity on the performance and flow field aerodynamics of vertical axis wind turbines at low Reynolds numbers. Renewable Energy 2016;92:474–83.
[43] Rezaeiha A, Montazeri H, Blocken B. Towards optimal aerodynamic design of vertical axis wind turbines: Impact of solidity and number of blades. Energy 2018;165:1129–48.
[44] Elsaka MM, Ingham DB, Ma L, Pourkashanian M. CFD analysis of the angle of attack for a vertical axis wind turbine blade. Energy Convers Manage 2019;182:154–65.